P 1.7 WHY THE MELTING LAYER REFLECTIVITY IS NOT BRIGHT AT 94-GHz

Pavlos Kollias[1] and Bruce Albrecht[2]

Brookhaven National Laboratory, Upton NY (1)
University of Miami, Miami FL (2)

1. INTRODUCTION

Early observations of stratiform rain from centimeter wavelength radars (e.g., Battan, 1973), revealed an area of enhanced radar reflectivity near the 0° C isotherm. The enhancement of the radar reflectivity at the melting layer captured the interest of radar meteorologists since the early days (e.g., Austin and Bemis, 1950) of radar meteorology (e.g., Aden and Kerker, 1951; Lhermitte and Atlas, 1963). The reflectivity enhancement was attributed to the melting of snowflakes and their conversion to raindrops, particles with higher dielectric constant. Furthermore, the increase of the fall velocity of the melted particles induces a reduction in the number of particles (divergence) and a small drop of the radar reflectivity. This shallow layer extends about 500-700 m below and it is called the radar "bright band".

The shape and intensity of the radar bright band is related to the shape and number concentration of the ice crystals and snowflakes above the melting layer, the melting rate of the snowflakes, their maximum size, and the rainfall intensity. But there has been no real appreciation for how wavelength influences the final shape of the radar reflectivity profile in the melting layer. This is exemplified in the case of 94-Ghz radars that use the shortest wavelength available for meteorological applications.

At 94-GHz, no radar bright band is observed (Fig. 1) at the melting layer. A sharp increase of the radar reflectivity is observed (e.g. Sassen et al., 2005) without a following decrease in the radar reflectivity. Often, at low rainfall rates, a small decrease (1-2 dBZ) of the radar reflectivity ("dark band") is observed first, just below the 0°C, before the sharp increase of the radar reflectivity is observed.

The aim of this study is to provide a comprehensive understanding of the 94-GHz radar profile in the melting layer (Fig. 1) through the use of a melting layer model and comparisons with collocated observations from vertically pointing 94- and 3-GHz radars in stratiform rain. We are particularly interested in explaining the lack of a reflectivity decrease at the base of the melting layer and investigate the conditions that could lead to the development of a shallow dark-band near the top of the melting layer.

Corresponding author's address: Brookhaven National Laboratory Earth Systems Science Division Bldg 490D, Bell Ave.Upton NY, 11973, email: ***pkollias@bnl.gov***

2. MODELING OF THE MELTING LAYER

Modeling efforts on the melting layer of precipitation abound in the literature, from one dimensional models (eg., Klassen, 1988; D' Amico, 1998), two dimensional (Szyrmer and Zawadski, 1999) and Doppler spectra (Skaropoulos and Russchenberg, 2003) models. Our aim is to analyze the radar profile of the melting layer, not the development of a new physical model of melting snowflakes. Thus, the physical model described in Szyrmer and Zawadski (1999) is used to provide the vertical profile of the melting hydrometeors needed for the radar forward model. The melting of snowflakes occurs in a shallow (500-700 m) layer below the 0°C isotherm where snowflakes melt and convert into raindrops. Above the melting layer (T < 0°C), the snowflakes are modeled as a mixture of ice and air (ice inclusions in air matrix), and the density of the snow determines the volume fraction f of the ice in the air. In our study, the $p_S(D_S)=0.015D_S^{-1}$ (Mitchell et al., 1990) was selected to describe the relationship of the snow density p_s to the diameter of the

snowflake D_s. In the melting layer, a mixture of partially melted snow particles and raindrops exist. The shape of the particles during the melting is highly variable (e.g., Willis and Heymsfield, 1989). In our study we have adopted three different melting snowflake models from Fabry and Szyrmer (1999):

Model 1: the melting hydrometeor is composed by ice inclusions in air matrix (snow) in a water matrix, [[[ice], air], water]
Model 2: the melting hydrometeor is composed by ice inclusions in a water matrix in an air matrix, [[[ice], water], air]
Model 3: the melting hydrometeor is composed by air inclusions in a matrix composed by a mixture of ice inclusions in a water matrix, [air, [[ice], water]]

For each melting hydrometeor model, the average dielectric constant of the uniform mixture (inclusion–matrix) is derived by the Maxwell Garnett formula (Maxwell Garnett, 1904; Bohren and Battan 1982; Meneghini and Liao, 2000). Once the dielectric constant of the spherical melting snowflakes is specified at each height step in the melting layer, the Mie scattering solution is used to calculate their scattering characteristics.

3. RESULTS

On July of 2002, NASA's CRYSTAL-FACE experiment for the study of tropical cirrus anvils took place in South Florida. During the experiment, the NOAA/AL 3-GHz profiler and the University of Miami 94-GHz Doppler cloud radar were collocated at a ground site 40 km southwest of Miami FL. Radar observations of the melting layer during a weak stratiform precipitation even at 94-GHz (Fig. 1) revealed the absent of an area of enhanced reflectivity (bright-band), the presence of a sharp increase in the reflectivity, and often the presence of a reflectivity minimum (dark-band) at the top of the melting layer. Fig. 2 shows the simulated radar reflectivity and attenuation at 94-GHz (top) for an exponential raindrop size distribution (Marshall and Palmer, 1948), a surface rainfall rate of 1 mmhr^{-1} and for all three melting snowflake models. For comparison, the corresponding profiles at 3-

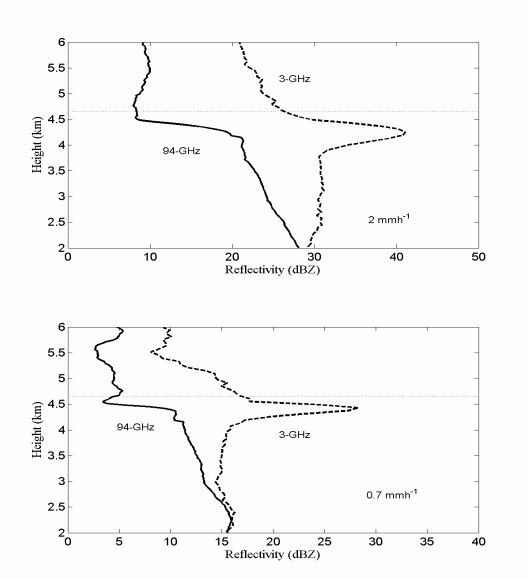

Fig. 1. Observed profiles of radar reflectivity at 3-GHz (dotted line) and 94-GHz (solid line) in stratiform precipitation. The 0° C isotherm is located at 4.6 km and the surface rainfall rate is 2 mmhr^{-1} (top) and 0.7 mmhr^{-1} (bottom). The 94-GHz reflectivity profile near the surface has been matched to the 3-GHz reflectivity values

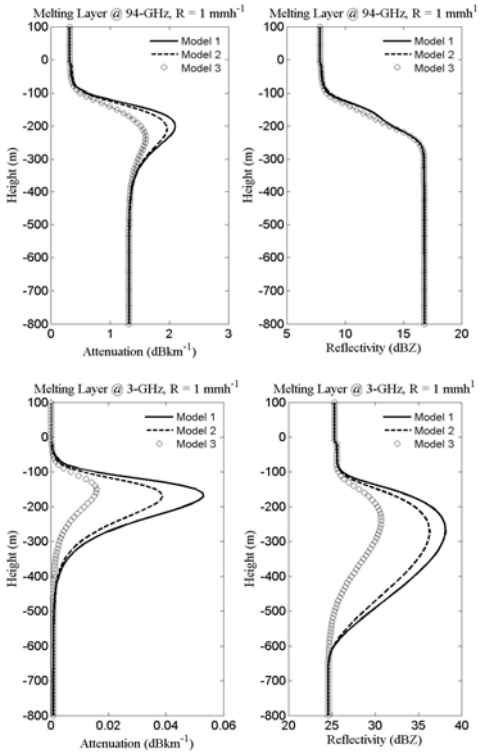

Fig. 2 Simulated profiles of radar reflectivity and attenuation at 94-GHz (top) and 3-GHz (bottom) for three different models of melting snowflakes (Fabry and Szyrmer, 1999) for a Marshall-Palmer raindrop size distribution and 1 mmhr^{-1} surface rainfall rate.

GHz are shown (Fig. 2, bottom). The simulations are in good agreement with the observations (Fig. 1). The melting layer ends at the depth of 630 m below the 0°C where the largest snowflake in the physical model completely melts to a spherical raindrop with 4 mm diameter. This is in good agreement with the 3-GHz radar reflectivity profile, but the 94-GHz reflectivity profile is invariant below 250 m depth and depend less on the melting snowflake model. The maximum attenuation simulated at 94-GHz in the melting layer is between 1.5-2.2 dBK^{-1} among the different melting snowflake models used, while the attenuation in the liquid layer is 1.3 dBK^{-1}. When averaged over the depth of the melting layer, the 94-GHz radar signal attenuation is comparable to the attenuation in the liquid layer below the melting layer. This is not the case at 3-GHz, where signal attenuation in the melting layer is much stronger than it is in the liquid layer (Fig. 2).

At 3-GHz the contribution from a certain size raindrop is proportional to D^6. As a result, few large raindrops in the radar resolution volume contribute to the Doppler moments as much as thousands of small raindrops. This is not valid in 94-GHz radars since the backscattering cross section for raindrops is not proportional to the sixth power of the raindrop diameter (Kollias et al., 2002). Fig. 3 shows the contribution to the reflectivity profiles of Fig. 2 from four raindrop size ranges: 0-1, 1-2, 2-3 and 3-4 mm for a Marshall-Palmer exponential size distribution (Marshall and Palmer, 1948) and 1 $mmhr^{-1}$ rainfall rate. At 94-GHz the class of raindrops with diameter less than1 mm is the dominant contributor to the final shape of radar profile shown in Fig. 2. The complete melting of the snowflake that converts to a 1 mm diameter raindrop occurs at 230 m depth and beyond this point the reflectivity profile at 94-GHz remains constant. Despite the melting of larger snowflakes and the creation of large raindrops deeper in the melting layer, their backscattering cross-section is not proportional to D^6 at 94-GHz; and if we account for the exponential drop of their number concentration (Marshall and Palmer, 1948), their contribution to the reflectivity profile is not significant. Thus there is no further increase of the reflectivity beyond the depth where the contribution from relatively small raindrops overwhelms the contribution from larger raindrops. Furthermore, there is no noticeable decrease in the reflectivity near the base of the melting layer when the fast falling large raindrops induce a reduction in the number of particles. This is not the case at 3-GHz. The contribution to reflectivity from large raindrops generated by the complete melting of snowflakes deep in the melting layer is proportional to D^6 and this high exponent overcomes the exponential drop in the number concentration. Thus, the overall effect is a significant contribution to the reflectivity profile from classes of large raindrops deep in the melting layer (Fig. 3, bottom) that affect the final shape of the reflectivity profile and are responsible for the presence of the radar bright-band.

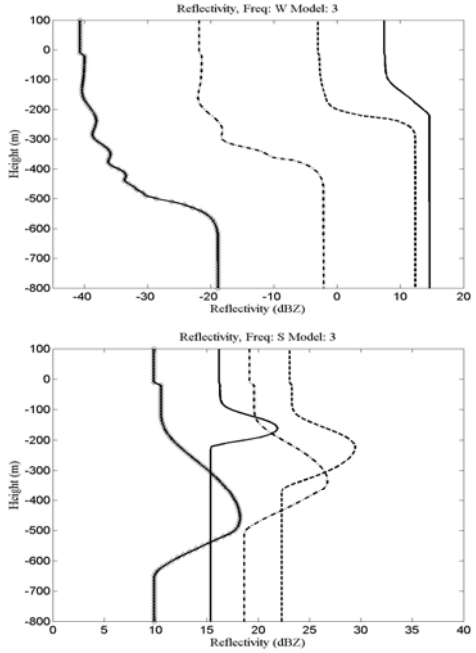

Fig. 3 Vertical profiles of radar reflectivity contribution from four raindrop size ranges: 0-1 mm (solid), 1-2 (dashed), 2-3 (dashed-dotted) and 3-4 (diamonds) for a Marshall-Palmer size distribution and 1 $mmhr^{-1}$ surface rainfall rate.

Another interesting feature observed (Fig. 1) is the presence of a shallow reflectivity minimum ("dark"-band) just below the 0°C. The examination of a large data set of 94-GHz radar observations of stratiform precipitation demonstrated that this narrow "dark" band is more pronounced during weak rainfall rates (less than 1 $mmhr^{-1}$). Furthermore, the simulations shown in Fig.2

show no evidence of reflectivity minimum just below the 0°C.

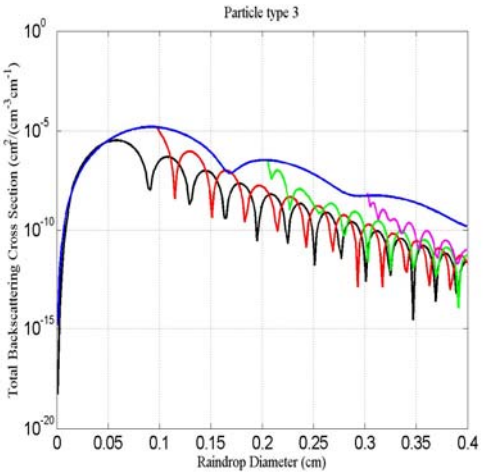

Fig. 4 Backscattering cross-section of hydrometeors multiplied by their number concentration at various depths in the melting layer as a function of their equivalent raindrop diameter: Top of the melting layer (no melting, black line), depth where 1 mm raindrop forms (red), depth where 2 mm raindrop forms (green), depth where 3 mm raindrop form (magenta) and base of the melting layer (all liquid, blue line).

During the melting process, there are two competing mechanisms that contribute to the backscattering cross-section of the melting snowflakes: The decrease of the diameter due to the collapse of the low-density snowflake to a raindrop decreases the backscattering, and the increase of the dielectric constant of the hydrometeor due to the presence of more water in the liquid phase increases the backscatter. Furthermore, the melting snowflakes have sizes comparable to the short wavelength λ = 3.2 mm (Mie scattering regime) and the backscattering cross-section as a function of the diameter exhibits a quasi-periodic form with an exponential damping of the oscillation (Fig. 4). The oscillating nature of the backscattering curve is caused by the superposition of the multipole terms described in the Mie scattering solution. Fig. 4 shows the backscattering cross-section of hydrometeors (for snowflake model 3) multiplied by their number concentration at various depths in the melting layer. It is apparent from Fig. 4 that certain sizes of snowflakes will undergo decreases in their backscattering cross-section during the melting process before they melt completely. Such behavior is evident for raindrop with diameters larger than 0.7 mm and only for certain size ranges of raindrops.

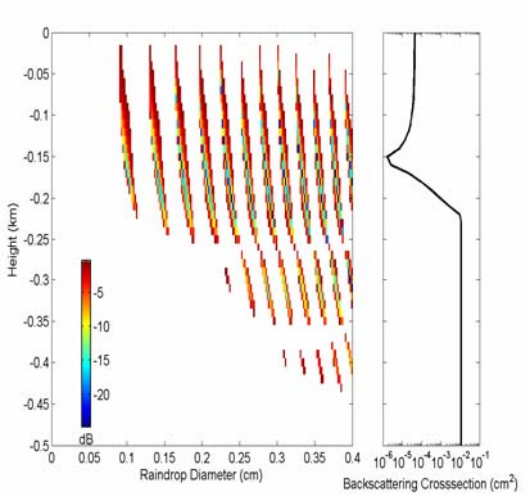

Fig. 5. Mapping of the parameter $10\log_{10}[cb_{min}(D)/cb_{snowflake}(D)]$, where $cb_{min}(D)$ is the minimum simulated backscatter cross-section of a particle with melted diameter D and $cb_{snowflake}(D)$ is the simulated backscatter cross-section of the snowflake with melted diameter D above the melting layer. The colored areas indicated depth and diameter ranges where the melted particle has lower backscatter cross section that its corresponding snowflake particle. The white area indicates depth and diameter ranges where the backscatter cross-section of the melting particle is higher that the backscatter cross-section of its corresponding snowflake above the melting layer. The backscattering cross-section of a melting snowflake with melted diameter 1 mm is shown on the right.

In Fig. 5 the backscattering minima occur near the top of the melting layer, which is in good agreement with the observations (Fig. 5). Small raindrops (D < 0.8 mm) do not contribute to the dark-band. In contrast, small raindrops form near the top of the melting layer and contribute to the large reflectivity increase observed and simulated (Fig. 2). Thus, these “localized” in diameter size and melting layer depth minima in the backscattering cross-section can affect the reflectivity profile near the top of the melting layer if small raindrops are in low concentrations.

4. SUMMARY

At 94-GHz, no radar bright band is observed. The melting of precipitating particles results in an abrupt increase in the radar reflectivity without a following

decrease at the base of the melting layer. In addition, a small decrease of the radar reflectivity ("dark" band) is often observed near the top of the melting layer. We investigate the scattering mechanism responsible for the observed structure of the 94-GHz radar reflectivity profile in the melting layer. The simulations presented in this study are in good agreement with the observations and capture the main features of the 94-GHz radar reflectivity profile in the melting layer. Small raindrops that are generated first, near the top of the melting layer through the melting of their corresponding snowflakes have an overwhelming effect on the reflectivity profile, contrary, to the insignificant effect of small raindrops at lower radar frequencies to the final shape of the reflectivity profile. Furthermore, during melting, certain size classes of snowflakes undergo a decrease of their backscattering cross-section, and if their concentration relative to the other snowflakes is high, then a dark band is produced near the top of the melting layer. Overall, low concentrations of small raindrops (D < 1 mm) are required for the generation of the radar dark band. The results from this study will improve our understanding of the melting layer radar signature at high radar frequencies, a critical issue for the development of new precipitation retrieval techniques from ground or space using cloud radars.

5. ACKNOWLEDGEMENT

This work was supported by NASA CRYSTAL-FACE Grant Number NAG511508 and NSF ATM 0201072.

6. REFERENCES

Aden A. I., and M. Kerker, 1951: Scattering of electromagnetic waves by two concentric spheres. *J. Appl. Physics*, **22**, 1242-1246

Austin P. M., and A. C. Bemis, 1950: A quantitative study of the "bright band" in radar precipitation echoes. *J. Meteor.*, **7**, 145-151

Battan, L. J., 1973: Radar Observations of the Atmosphere. Univ. of Chicago Press, pp 325.

Bohren, C. F., and L. J. Battan, 1982: Radar backscattering of microwaves by spongy ice spheres. *J. Atmos. Sci.*, **39**, 2623-2628.

D'Amico, M., A. R. Holt, and C. Capsoni, 1998: An anisotropic model of the melting layer. *Radio Sci.*, **33**, 535-552.

Doviak, R. J., and D. S. Zrnic, 1993: Doppler Radar and Weather Observations, Academic Press, pp 562.

Fabry, F., and W. Szymer, 1999: Modeling of the melting layer. Part II: Electromagnetic. *J. Atmos. Sci.*, **56**, 3593-3600.

Joss, J., E. G. Gori., 1978: Shapes of Raindrop Size Distributions**.** *J. Appl. Meteor.* **17**, 1054–1061.

Klaassen, W., 1988: Radar observations and simulations of the melting layer of precipitation. *J. Atmos. Sci.*, **45**, 3741-3753.

Kollias, P., B.A. Albrecht, and F. D. Marks, Jr., 2002: Why Mie? Accurate observations of vertical air velocities and rain drops using a cloud radar. *Bull. Amer. Met. Soc.,* 83, 1471-1483.

Lhermitte, R.M. and D. Atlas, 1963. Doppler fall speed and particle growth in stratiform precipitation. Proc. Tenth Wea. Radar Conf., Boston, Am. Meteor. Soc., 297-302.

Marshall, J. S., and W. H. Palmer, 1948: The distribution of raindrops with size. *J. Meteor.,* 5, 165–166.

Maxwell Garnett, J. C., 1904: Colours in metal glasses and in metallic films. *Philos. Trans. Roy. Soc. London*, **203A**, 385-420.

Meneghini, R., and L. Liao, 2000: Effective Dielectric Constants of Mixed-Phase Hydrometeors. *J. Atmos. Oceanic. Tech.*, **17**, 628-640.

Mitchell, D. L., R. Zhang, and R. L. Pitter, 1990: Mass-dimensional relationships for ice particles and the influence of riming on snowfall rates. *J. Appl. Meteor.*, **29**, 153-163.

Sassen, K., J. R. Campbell, J., Zhu, P. Kollias, M. Shupe and C. Williams. 2005: Lidar and Triple-Wavelength Doppler Radar Measurements of the Melting Layer: A Revised Model for Dark- and Brightband Phenomena**.** *J. Applied. Meteor.* **44**, 301-312

Skaropoulos, N. C., and H. W. J. Russchenberg, 2003: Simulations of Doppler spectra in the melting layer of precipitation. *Geoph. Res. Letters*, *DOI 10.1029/2003GL016959*

Szyrmer W., and I. Zawadski, 1999: Modeling of the melting layer. Part I: Dynamics and microphysics. *J. Atmos. Sci.*, **56**, 3573-3592.

Willis, P. T., A. J. Heymsfield, 1989: Structure of the melting layer in mesoscale convective system stratiform precipitation. *J. Atmos. Sci.*, **46**, 2008-2025.